

4-1-2002

Direct observation of magnetic domains in phase separated Nd_{0.7}Ca_{0.3}MnO₃ single crystals

Xiaojuan Fan

Marshall University, fan2@marshall.edu

Hideomi Koinuma

Tetsuya Hasegawa

Follow this and additional works at: http://mds.marshall.edu/physics_faculty



Part of the [Physics Commons](#)

Recommended Citation

Fan, X., Koinuma, H., & Hasegawa, T. (2002). Direct observation of magnetic domains in phase separated Nd_{0.7}Ca_{0.3}MnO₃ single crystals. *Physical Review B*, 65(14), 144401.

This Article is brought to you for free and open access by the Physics at Marshall Digital Scholar. It has been accepted for inclusion in Physics Faculty Research by an authorized administrator of Marshall Digital Scholar. For more information, please contact zhangj@marshall.edu.

Direct observation of magnetic domains in phase separated $\text{Nd}_{0.7}\text{Ca}_{0.3}\text{MnO}_3$ single crystals

Xiao-Juan Fan,¹ Hideomi Koinuma,^{1,2} and Tetsuya Hasegawa^{1,2}

¹*Advanced Materials Laboratory, National Institute for Materials Science, Tsukuba 305-0044, Japan*

²*Materials and Structures Laboratory, Tokyo Institute of Technology, Yokohama 226-8503, Japan*

(Received 7 September 2001; published 8 March 2002)

The magnetic properties of single-crystalline $\text{Nd}_{0.7}\text{Ca}_{0.3}\text{MnO}_3$ were studied with both macroscopic and microscopic probes. The magnetization shows large irreversibility behavior between zero-field-cooled and field-cooled data at low field, suggesting a phase separation driven by competition between ferromagnetic and antiferromagnetic phases. The scanning superconducting quantum interference device microscope observations under zero field gave clear evidence that the compound includes ferromagnetic regions as the ground state below T_c . It was also found that two different phase-separated states appear, depending on temperature. At $T \sim 125$ K, weak but finite spontaneous magnetization develops, while the magnetization is abruptly enhanced below 95 K, possibly reflecting an increase of the volume fraction of the ferromagnetic region. The present results support the phase separation scenario that fine ferromagnetic particles embedded in an antiferromagnetic matrix are magnetostatically coupled to each other to form a network of macroscopic sizes.

DOI: 10.1103/PhysRevB.65.144401

PACS number(s): 75.30.Vn, 71.27.+a, 71.28.+d, 75.25.+z

Colossal magnetoresistance (CMR) of hole-doped perovskite manganese oxides has regained much attention since the discovery of a large decrease in resistance around the Curie temperature T_c , so-called negative CMR.¹⁻⁵ The parent member $R\text{MnO}_3$ (R is trivalent rare-earth ions), being a typical Mott insulator, possesses Mn^{3+} ions with the electronic configurations of $t_{2g}^3 e_g^1$ and a full spin $S=2$. As one introduces holes by partially substituting trivalent rare-earth ions with divalent alkaline-earth metals, the e_g^1 electrons become mobile and easily hop between the spin-aligned Mn^{3+} and Mn^{4+} ions through oxygen ions. This Zener's double-exchange (DE) mechanism⁶ gives rise to the conductivity and ferromagnetism (FM) in these systems. However, Millis *et al.*⁷ pointed out that the lattice polaron effect also plays an important role in the CMR phenomenon, due to the strong electron-phonon interaction coming from the Jahn-Teller distortion. The lattice distortion can be strongly controlled by the chemical pressure generated by A -site substitution with ions of different radii. Hwang *et al.*³ demonstrated that smaller A -site ions with an average radius $\langle r_A \rangle$ substantially enhance lattice distortion, which is responsible for the high resistivity and low Curie temperature.

One fascinating feature of these manganese oxides is the electronic phase separation (PS) into different magnetic phases, driven by a strong coupling between spin, charge, and lattice degrees of freedom. The length scale of the magnetic inhomogeneity reported so far shows wide scattering range from subnanometer to micron.⁸ Complex spin alignments were also observed in charge- and orbital-order (CO and OO, respectively) systems, such as $\text{La}_{1/2}\text{Ca}_{1/2}\text{MnO}_3$,^{9,10} where the CO antiferromagnetic (AFM) coupling competes with the DE-FM ones, giving rise to the transition from FM to AFM in low- T regions. Very recently, Deac *et al.*¹¹ reported that $\text{Pr}_{1-x}\text{Ca}_x\text{MnO}_3$ displays an unconventional spin-glass-like PS in which ferromagnetic clusters are postulated to disperse in a nonferromagnetic insulating matrix and concluded that the FM insulating state appears only under external fields. Another study by Yoshizawa *et al.* revealed un-

usual irreversible behavior in $\text{Pr}_{0.7}\text{Ca}_{0.3}\text{MnO}_3$, suggesting that excess Mn^{3+} ions are randomly localized, which obviously favors spin-glass-like model.^{12,13} Based on neutron scattering, muon spin relaxation, neutron diffraction, calorimetric, and magnetic measurements, several other authors claimed that the FM and AFM regions spatially coexist in $\text{Pr}_{0.7}\text{Ca}_{0.3}\text{MnO}_3$, resulting in a "frustrated" history-dependent magnetization.¹⁴⁻¹⁶ This magnetic relaxation process was thought to come from the competition between FM and AFM interactions which are induced by the DE and superexchange mechanisms, respectively. In contrast to the (Pr,Ca)-based compounds with relatively smaller $\langle r_A \rangle$, larger $\langle r_A \rangle$ systems, such as (La, Sr)-based perovskite with a $\text{Mn}^{3+}/\text{Mn}^{4+}$ ratio of 7/3, stabilize the FM metallic state even around room temperature,⁵ which is well understandable in the framework of DE scenario. Therefore, detailed investigations of the electronic PS phenomena in a variety of compounds with different $\langle r_A \rangle$ values help us to understand an overview of electronic natures in doped manganese perovskites.

In this paper, we report the results of magnetic measurements on $\text{Nd}_{0.7}\text{Ca}_{0.3}\text{MnO}_3$ single crystals with a very small $\langle r_A \rangle$ value ~ 1.168 Å and tolerance factor $t \sim 0.924$. The bulk magnetization measurements revealed spin-glass-like behavior at low temperatures. A spontaneous long-range ferromagnetic order was also observed by a scanning superconducting-quantum-interference-device (SQUID) microscope (SSM) under zero magnetic field below T_c . The relative magnitude of spontaneous magnetization decreases as increasing temperature. We also found the two different transitions, which seems to correspond to the anisotropic reorientation of spins within ferromagnetic clusters and the reduction of the volume of FM clusters, respectively. The present observations suggest the scenario of the phase separation that fine FM domains are embedded in AFM matrix.

Single crystals of $\text{Nd}_{0.7}\text{Ca}_{0.3}\text{MnO}_3$ were grown by the floating zone method in pure O_2 atmosphere. Stoichiometric quantities of Nd_2O_3 , CaCO_3 , and Mn_3O_4 were mixed, sin-

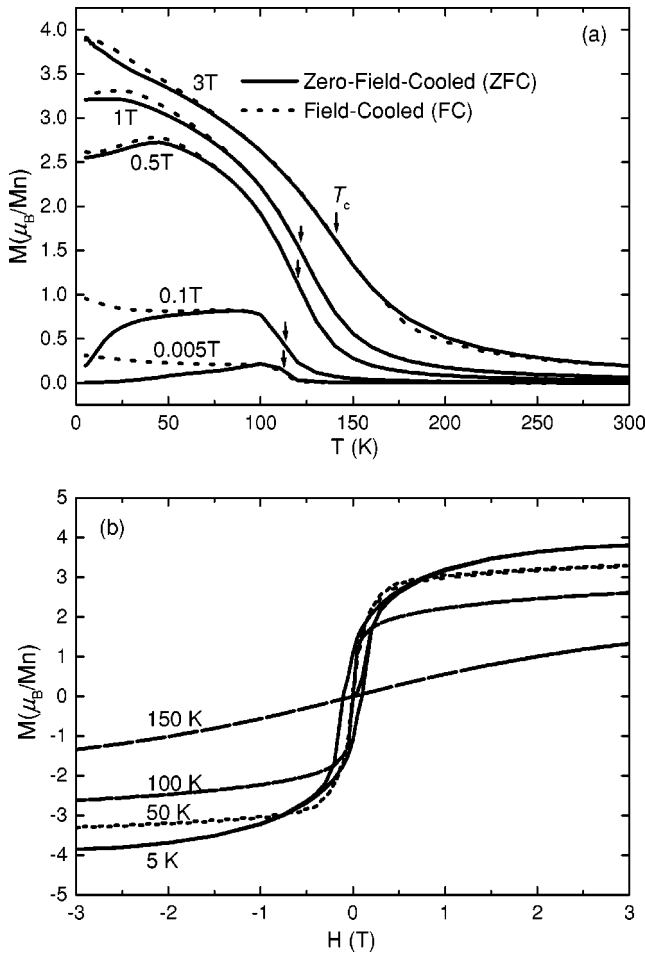


FIG. 1. (a) Zero-field-cooled (ZFC) and field-cooled (FC) magnetization as a function of temperature at different fields. T_c is indicated by arrows. (b) Field dependence of the magnetization at different temperatures.

tered at 1300 °C for 20 h three times with intermediate re-grinding, pressed into a rod of $\phi 5 \times 8$ mm, and finally sintered in air at 1350 °C. The melting zone was vertically scanned at a speed of 3–5 mm/h, and the seed and feed rods were rotated in opposite directions at a relative rate of 50 rpm. The middle of the as-grown crystal was cut into a rectangular shape for measurements.

Bulk magnetizations at temperature range from 5 to 300 K and external field up to 5 T were measured using a conventional SQUID magnetometer. Temperature dependences of the magnetic domain structures were imaged with a SSM at zero field. The microscope has a spatial resolution of ~ 5 μm and a very high field sensitivity of ~ 10 nT.^{17–19}

The dc magnetization measurements were performed in the zero-field-cooled (ZFC) and field-cooled (FC) conditions, as shown in Fig. 1(a). On lowering the temperature, the magnetizations show a steep rise below the critical temperature T_c of 109 K, 110 K, 119 K, 120 K, and 140 K for applied fields of 0.005 T, 0.1 T, 0.5 T, 1 T, and 3 T, respectively, corresponding to the onset of ferromagnetism. Here, we defined T_c as the peak position in the dM/dT vs T curve. Notably, T_c shifts to the higher-temperature side with in-

creasing magnetic field, possibly reflecting that the spins in FM clusters are sensitively reoriented or the FM clusters are enlarged by the external field. Another interesting feature in the M - T curves is the strong history dependence of the magnetization at low fields. Namely, the ZFC and FC magnetization curves differ from each other below a critical temperature T_{irr} , which has been argued as a characteristic behavior of both spin-glass and inhomogeneous clustered systems, arising from the competition of two different microscopic interactions. We found that the irreversibility appears just below the FM transition temperature T_c , contrary to the conventional spin-glass case,²⁰ where the FC-ZFC irreversibility occurs significantly below T_c . This suggests that the present system cannot be explained by the simple paramagnetic spin-glass model but includes phase separation into FM and AFM regions in a microscopic sense. Some early studies of $\text{Pr}_{0.7}\text{Ca}_{0.3}\text{MnO}_3$ (Ref. 11) and $\text{SmNi}_{0.3}\text{Co}_{0.7}\text{O}_3$ (Ref. 21) observed similar behavior, which has been attributed to the coexistence of FM and AFM phases.

Large irreversibility at $H \leq 0.1$ T is understandable by assuming that the moments of FM domains are randomly orientated in the ZFC case, while they tend to point toward to a preferred direction in the FC case.²² This implies that either intracluster or intercluster FM coupling may overcome the influence of such low external fields. In addition, it should be pointed that in the present field range T_{irr} is almost identical to the peak temperature T_p of ZFC magnetization. This relatively small and constant interval $\Delta T = T_{irr} - T_p$ as increasing field presumably indicates that the FM clusters maintain their sizes uniform,²³ but the alignment of their moments is responsible for the increased magnetization. With further increasing magnetic field, T_p rapidly decreases and disappears for $H = 3$ T. But the magnitude of initial magnetization dramatically increases, and the ZFC and FC curves show less difference with increasing field, possibly because that the FM phase becomes majority overwhelming the minority AFM one.

The magnetization versus field curves at different temperatures are plotted in Fig. 1(b). Magnetization curves below T_c are saturated at high field due to the domain rotations of the FM clusters. The curve of 5 K shows a large hysteresis behavior and the saturated magnetization of $\sim 4\mu_B$, which is fairly larger than the full moment of Mn ions, $3.7\mu_B$. This gives clear evidence that the magnetization partially comes from the Nd sublattice. A specific-heat study of $\text{Nd}_{0.67}\text{Sr}_{0.33}\text{MnO}_3$ reported the similar result that the Nd moments induced by the Nd-Mn interaction also contribute to the magnetization at low temperature.²⁴ At $T = 50$ K, 100 K, hysteresis is not discernible, but the magnetizations still indicate a Z-shaped H dependence at high field, which is a signature of ferromagnetic order.²⁵ At $T = 150$ K above T_c , the M - H relation is almost linear with a slight downward curvature at higher fields, being consistent with the Brillouin behavior of a paramagnetic material.

In order to map the microscopic magnetic structure of $\text{Nd}_{0.7}\text{Ca}_{0.3}\text{MnO}_3$ without an external field, we performed the SSM measurements at the temperature range of 3–127 K. It should be stressed here that SSM less disturbs the magnetic

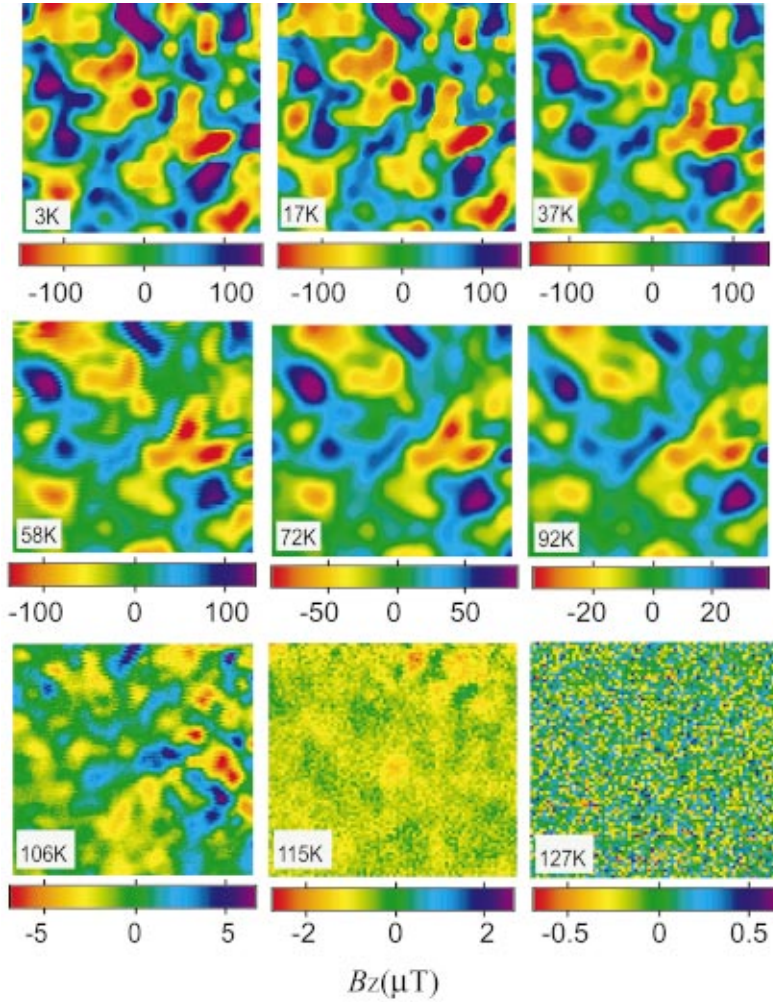


FIG. 2. (Color) Scanning SQUID images of $\text{Nd}_{0.7}\text{Ca}_{0.3}\text{MnO}_3$ single crystal at different temperatures. The image sizes are $800 \mu\text{m} \times 800 \mu\text{m}$. The color bars indicate the B_z scales in units of μT .

structures of specimens, compared with magnetic force microscope (MFM) utilizing a ferromagnetic cantilever. Figure 2 shows the magnetic images obtained at various temperatures. The color bar indicates the measured magnetic field perpendicular to the sample surface, B_z . From the images, one can clearly see magnetic domains with dimensions of tens to hundreds of micrometers, which are significantly larger than the length scale of electronic PS previously reported.⁸ We speculate that the present compound contains FM droplets smaller than the spatial resolution of the SQUID sensor, but their magnetic moments tend to align to form domains of macroscopic sizes due to the magnetostatic interaction between them. The domain size seems unchanged with temperature below 92 K, but the B_z value quickly decreases, particularly round 92 K. Above 92 K, smaller domains with much lower B_z were observed, and domains eventually disappear at $T \sim 127$ K.

In Fig. 3, we plot the maximum B_z value obtained from each magnetic image in Fig. 2, $B_{z\text{max}}$, against temperature. Surprisingly, the $B_{z\text{max}}(T)$ curve can be divided into two parts: region I ($T \leq T_{c1} \sim 95$ K) and region II ($T_{c1} \leq T \leq T_{c2} \sim 125$ K), where T_{c1} and T_{c2} correspond well to the irreversible point and the onset of magnetization in the M - T curve, respectively. In general, the decrease in $B_{z\text{max}}$ is attributable to the reduction of either M or the domain size. As

is well known, the magnetization of a ferromagnet can be expressed by the Brillouin function,

$$\frac{M}{M_s} = \frac{2J+1}{2J} \coth \frac{2J+1}{2J} \alpha - \frac{1}{2J} \coth \frac{1}{2J} \alpha,$$

where $\alpha = Jg\beta(H+NM)/kT$, J is the angular momentum, and M_s is the saturated magnetic moment at zero temperature. In region I, the overall feature of $B_{z\text{max}}(T)$ was well described by the Brillouin function assuming $T_c = 95$ K, while the domain size is almost temperature independent, as already pointed out. These facts strongly suggest that the volume fraction of FM phase is essentially unchanged with temperature and that the decrease of magnetization is associated with the reorientation of moments due to thermal fluctuation. It is also notable that the M - T curve reveals irreversibility in this temperature range. The $B_{z\text{max}}(T)$ curve at low temperatures is rather consistent with the Bloch's $T^{3/2}$ law based on spin-wave theory, $M(T) = M(0)[1 - AT^{3/2}]$, as shown in the inset of Fig. 3. This implies that the magnon excitation largely contributes to the magnetization at finite temperatures in the present material. In region II, in contrast, domains have smaller sizes with relatively lower B_z , which diminishes to zero at $T = T_{c2}$. More interestingly, irreversibility disappears on the M - T plot at this temperature range. These distinctive

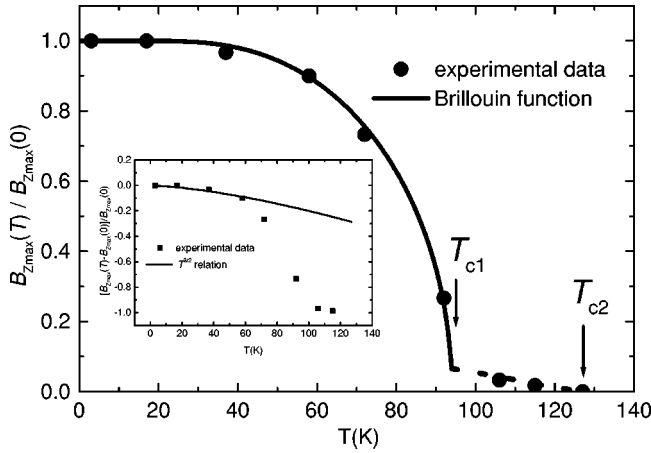


FIG. 3. Maximum field B_{zmax} obtained from the scanning SQUID image as a function of temperature. The solid line denotes the Brillouin function with $T_c = 95$ K. The dotted line is a guide for the eye for the experimental data at $T_{c1} \leq T \leq T_{c2}$. The inset shows Bloch's $T^{3/2}$ function fitted to the experimental B_{zmax} below 60 K.

differences between regions I and II imply that the pattern of electronic PS drastically changes at $T = T_{c1}$. The similar situation, i.e., two different T_c values, was also encountered in the MFM investigations of $\text{La}_{1-x}\text{Sr}_x\text{MnO}_3$ ($x=0.3$) film.²⁶

The large irreversible behavior in region I is thought to be due to the competition of two different microscopic interactions with roughly equal strengths. In other words, the competition comes from FM and AFM regions with comparable volume fractions. Obviously, region II without irreversibility

does not fall under this category. Considering from the facts that region II shows lower B_{zmax} and smaller domain sizes, two possibilities can be assumed. First, small fractions of the FM phase appear in the AFM matrix at $T = T_{c2}$, but the AFM phase is still dominant. At $T = T_{c1}$, the second transition sets in, and the volume fraction of FM domains enlarges abruptly and becomes comparable to that of AFM one. The second possibility is that AFM spins start to cant at $T = T_{c2}$, gradually forming a spatially distributed network of canted moments. Although the gross magnetization associated with canted spin is relatively low, the SQUID sensor used here has sufficiently high magnetic sensitivity to detect it.¹⁸ For further understanding the origin of transitions at T_{c1} and T_{c2} , more detailed studies of magnetic domains using a higher-spatial-resolution probe are needed.

In summary, we have shown strong evidence that (Nd,Ca)-based manganite at $x=0.3$ could be a typical example of PS system in transition-metal oxides. The large irreversibility between the ZFC and FC magnetization data at low fields indicates that FM and AFM phases of comparable volume fractions compete with each other to produce an inhomogeneous PS phase. Even in the absence of an external field, we have directly observed magnetic domains originating from fine FM regions with a scanning SQUID microscope. From the SSM results, we found two magnetic transitions at $T = T_{c1}$ and $T = T_{c2}$; at $T = T_{c2}$ spontaneous magnetization appears, while below T_{c1} the observed B_z rapidly grows, following the Brillouin relation. These observations suggest that the spatial PS pattern is drastically rearranged at T_{c1} and the AFM phase becomes dominant for $T > T_{c1}$.

- ¹K. Chahara *et al.*, Appl. Phys. Lett. **63**, 1990 (1993); R. von Helmlolt *et al.*, Phys. Rev. Lett. **71**, 2331 (1993).
- ²S. Jin, T. H. Tiefel, M. McCormack, R. A. Fastnacht, R. Remesh, and L. H. Chen, Science **264**, 413 (1994); A. P. Ramirez, J. Phys.: Condens. Matter **9**, 8171 (1997).
- ³H. Y. Hwang, S.-W. Cheong, P. G. Radaelli, M. Marezio, and B. Batlogg, Phys. Rev. Lett. **75**, 914 (1995).
- ⁴P. Schiffer, A. P. Ramirez, W. Bao, and S.-W. Cheong, Phys. Rev. Lett. **75**, 3336 (1995).
- ⁵Y. Tokura, Y. Tomioka, H. Kuwahara, A. Asamitsu, Y. Moritomo, and M. Kasai, J. Appl. Phys. **79**, 5288 (1996).
- ⁶C. Zener, Phys. Rev. **82**, 403 (1951); P. W. Anderson and H. Hasegawa, *ibid.* **100**, 675 (1955).
- ⁷A. J. Millis, P. B. Littlewood, and B. I. Shraiman, Phys. Rev. Lett. **74**, 5144 (1995).
- ⁸J. M. De Teresa *et al.*, Nature (London) **386**, 256 (1997); M. Fath *et al.*, Science **285**, 1540 (1999); M. Hennion *et al.*, Phys. Rev. Lett. **81**, 1957 (1998); S. H. Chun, M. B. Salamon, Y. Tomioka, and Y. Tokura, Phys. Rev. B **61**, R9225 (2000); M. Uehara, S. Mori, C. H. Chen, and S.-W. Cheong, Nature (London) **399**, 560 (1999).
- ⁹E. O. Wollan and W. C. Koehler, Phys. Rev. **100**, 545 (1955); J. B. Goodenough, *ibid.* **100**, 564 (1955).
- ¹⁰P. G. Radaelli, D. E. Cox, M. Marezio, S.-W. Cheong, P. E. Schiffer, and A. P. Ramirez, Phys. Rev. Lett. **75**, 4488 (1995).
- ¹¹I. G. Deac, J. F. Mitchell, and P. Schiffer, Phys. Rev. B **63**, 172408 (2001).
- ¹²H. Yoshizawa, H. Kawano, Y. Tomioka, and Y. Tokura, J. Phys. Soc. Jpn. **65**, 1043 (1996).
- ¹³H. Yoshizawa, H. Kawano, Y. Tomioka, and Y. Tokura, Phys. Rev. B **52**, R13 145 (1996).
- ¹⁴P. G. Radaelli, G. Innonone, D. E. Cox, M. Marazio, H. Y. Hwang, and S.-W. Cheong, Physica B **241-243**, 295 (1998).
- ¹⁵S. Katano, J. A. Fernandez-Baca, and Y. Yamada, Physica B **276-278**, 787 (2000).
- ¹⁶C. Frontera, J. L. Garcia-Munoz, A. Llobet, M. Respaud, J. M. Broto, J. S. Lord, and A. Planes, Phys. Rev. B **62**, 3381 (2000).
- ¹⁷T. Morooka, S. Nakayama, A. Odawara, M. Ikeda, S. Tanaka, and K. Chinone, IEEE Trans. Appl. Supercond. **9**, 3491 (1991).
- ¹⁸T. Fukumura, M. Ohtani, M. Kawasaki, Y. Okimoto, T. Kageyama, T. Koida, T. Hasegawa, Y. Tokura, and H. Koinuma, Appl. Phys. Lett. **77**, 3426 (2000).
- ¹⁹Y. Matsumoto, M. Murakami, T. Shono, T. Hasegawa, T. Fukumura, M. Kawasaki, P. Ahmet, T. Chikyow, S. Koshihara, and H. Koinuma, Science **291**, 854 (2001).
- ²⁰J. E. Greedan, N. P. Raju, A. Maignan, Ch. Simon, J. S. Pedersen, A. M. Niraimathi, E. Gmelin, and M. A. Subramanian, Phys. Rev. B **54**, 7189 (1996).

- ²¹J. Pérez, J. García, J. Blasco, and J. Stankiewicz, Phys. Rev. Lett. **80**, 2401 (1998).
- ²²Z. Zeng, M. Greenblatt, and M. Croft, Phys. Rev. B **63**, 224410 (2001).
- ²³L. C. C. M. Nagamine, B. Mevel, B. Dienty, B. Rodmacq, J. R. Regnard, C. Revenant-Brizard, and I. Manzini, J. Magn. Magn. Mater. **195**, 437 (1999).
- ²⁴J. E. Gordon, R. A. Fisher, Y. X. Jia, N. E. Phillips, S. F. Reklis, D. A. Wright, and A. Zettl, Phys. Rev. B **59**, 127 (1999).
- ²⁵J. J. Neumeier and J. L. Cohn, Phys. Rev. B **61**, 14 319 (2000).
- ²⁶Y. -A. Soh, G. Aeppli, N. D. Mathur, and M. G. Blamire, J. Appl. Phys. **87**, 6743 (2000).